Silicon photonic crystal cavity enhanced second-harmonic generation from monolayer $WSe_2$



2017 2D Mater. 4 015031

(http://iopscience.iop.org/2053-1583/4/1/015031)

2D Materials

RECEIVED
12 July 2016

REVISED
1 November 2016

ACCEPTED FOR PUBLICATION
21 November 2016

PUBLISHED
7 December 2016

PAPER

# Silicon photonic crystal cavity enhanced second-harmonic generation from monolayer $WSe_2$

Taylor K Fryett[1], Kyle L Seyler[2], Jiajiu Zheng[1], Chang-Hua Liu[2], Xiaodong Xu[2,3,4] and Arka Majumdar[1,2,4]

1 Electrical Engineering, University of Washington, Seattle, WA-98195, USA
2 Physics, University of Washington, Seattle, WA-98195, USA
3 Material Science and Engineering, University of Washington, Seattle, WA-98195, USA
4 Author to whom any correspondence should be addressed.

**E-mail:** xuxd@uw.edu and arka@uw.edu

**Keywords:** 2D materials, nonlinear optics, photonic crystal cavity

Supplementary material for this article is available online

## Abstract

Nano-resonators integrated with two-dimensional materials (e.g. transition metal dichalcogenides) have recently emerged as a promising nano-optoelectronic platform. Here we demonstrate resonator-enhanced second-harmonic generation (SHG) in tungsten diselenide using a silicon photonic crystal cavity. By pumping the device with ultrafast laser pulses near the cavity mode at the telecommunication wavelength, we observe a near visible SHG with a narrow linewidth and near unity linear polarization, originated from the coupling of the pump photon to the cavity mode. The observed SHG is enhanced by factor of ~200 compared to a bare monolayer on silicon. Our results imply the efficacy of cavity integrated monolayer materials for nonlinear optics and the potential of building a silicon-compatible second-order nonlinear integrated photonic platform.

## 1. Introduction

Nonlinear integrated photonics plays a crucial role in building all-optical information processors [1, 2] and novel on-chip light-sources [3]. However, the weak optical nonlinearity of existing material systems results in large optical switching power, rendering optical information processing unattractive. The key to lower the required optical power is to incorporate nonlinear materials onto a nano-scale high quality factor ($Q$) resonator, where light can be stored in a small volume ($V_m$) and for an extended period of time [4]. It can be shown that for a nonlinear optical switch, the switching power scales as $V_m/Q^2$ for the third order and $V_m/Q^3$ for the second order nonlinearity [5]. This stronger dependence on cavity $Q$, along with a larger value of second-order $\chi^{(2)}$ nonlinear coefficients compared to $\chi^{(3)}$ coefficients, make $\chi^{(2)}$ nonlinear processes more suitable to realize low-power nonlinear optical devices. Unfortunately, silicon lacks the desired $\chi^{(2)}$ nonlinearity due to its centrosymmetric crystal structure; thus devices based on $\chi^{(3)}$ processes dominate current efforts in nonlinear integrated photonics [3, 6, 7]. While materials with large $\chi^{(2)}$ nonlinearities, such as III–V materials [8] are well-studied, their incompatibility with current CMOS foundries [9] hinders the scalability sought by the integrated photonics community. This is further exacerbated by the fact that deposition of high refractive index III–V materials on silicon changes the optical mode profile significantly, making the phase matching condition more difficult to satisfy. Researchers have also studied aluminum nitride for nonlinear optics [10] and have integrated it on silicon for electro-optic signal processing [11]. However, nonlinear optics with aluminum nitride integrated on a silicon-compatible platform has not yet been reported. A hybrid platform, where we can exploit the scalability provided by silicon photonics as well as realize strong $\chi^{(2)}$ nonlinearity, will be highly attractive for integrated nonlinear nano-photonics with applications to all-optical signal processing.

The recently discovered atomically thin 2D transitional metal dichalcogenides (TMDCs with chemical formula $MX_2$) [12] offer extraordinarily large second-order nonlinear coefficients [13, 14]. They can be easily integrated onto silicon devices by simple van der Waals bonding without the need of lattice matching

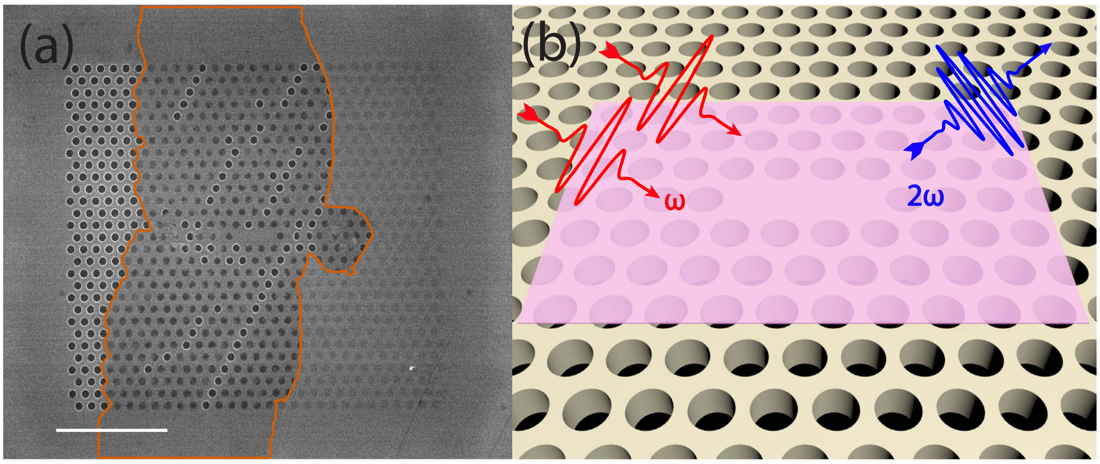


**Figure 1.** The fabricated device: (a) Scanning electron micrograph of the fabricated silicon photonic crystal cavity with monolayer $WSe_2$ on top, indicated by the orange outline. Visible stripes of holes inside the monolayer region are due to ripped monolayer during exfoliation. Scale bar: 10 $\mu$m. (b) Schematic of the device operation: two infrared (IR) photons denoted by the red Gaussian profiles with frequency $\omega$ resonantly couple into the photonic crystal cavity. The cavity mode interacts with the $WSe_2$ (the transparent pink sheet) which then generates the second harmonic photon at a frequency of $2\omega$, denoted by the blue Gaussian profile.

[15]. In spite of their atomically-thin thickness and evanescent coupling with the light, the effective nonlinearity offered by TMDC-integrated nano-resonator is comparable to that offered by a resonator completely made out of a $\chi^{(2)}$ nonlinear III–V material [16]. Cavity-enhanced second-order nonlinear optics with TMDCs has recently been observed in distributed Bragg reflector cavities [17, 18] and plasmonic resonators [19]. However, both of these cavity systems are unsuitable for low power operation due to their large mode volume and high loss (low Q), respectively. In this paper, we report the enhanced second-harmonic generation (SHG) of a tungsten diselenide ($WSe_2$) monolayer integrated on a planar silicon photonic crystal linear defect cavity, under ~1550 nm laser excitation. The choice of photonic crystal cavity (PCC) is largely motivated by its both small mode volume and high Q [20]. This is particularly important for using exfoliated TMDC monolayers as the modal overlap with the TMDC is further limited by the exfoliated sample size. The choice of the $WSe_2$ is primarily motivated by its high second-order nonlinearity near 1550 nm, the wavelength of interest for telecommunication. We measured a cavity enhancement of SHG by a factor of 200, which can be potentially further enhanced by switching to a wide band-gap substrate, such as silicon nitride, and using a resonator with modes at both the fundamental and second-harmonic frequency.

## 2. Methods

Preparation of the TMDC-cavity device largely followed the standard cavity fabrication and 2D material preparation processes [20–22]. A modified three-hole linear defect (L3) photonic crystal cavity (PCC) [23] is fabricated in a standard 220 nm thick silicon on insulator (SOI) wafer with a lattice periodicity of 398 nm and a radius of 116 nm. We patterned a 250 nm ZEP 520A mask using a 100 kV JEOL JBX6300FS electron beam lithography system. The mask was then transferred onto the silicon by using a chlorine ICP-RIE dry etching recipe followed by an undercutting step using a 1:10 solution of buffered oxide etchant. In parallel to the cavity fabrication, we exfoliated a monolayer $WSe_2$ onto a 300 nm $SiO_2$ on Si wafer. The monolayer was subsequently transferred onto the cavity using a dry transfer method [24]. Figure 1(a) shows the scanning electron micrograph of an integrated monolayer $WSe_2$ on silicon cavity device.

The cavity modes were identified before and after monolayer transfer using cross-polarized reflectivity measurements (see supplement) [25]. We found several cavity modes in the pristine cavity, including the fundamental mode at 1557 nm with a Q factor of ~10 000 (see supplement). Unfortunately, this high Q mode disappeared after the $WSe_2$ transfer. We have observed severe degradation of high-Q modes in several TMDC-PCC devices. Along with the fundamental mode, we also found several higher-order modes for both the pristine cavity and the 2D integrated cavity (figure 2(a)). The asymmetry in the measured resonance is primarily due to the Fano-type interference that happens as the cross-polarization is not perfect. Exact correspondence between these modes cannot be established with certainty, as the effect of monolayer transfer is not clear. However, the range of quality factor decreased from Q ~ 2000–3000 of the pristine cavity to ~700–800 after $WSe_2$ integration. The degradation of the cavity Q-factor is expected due to the residual loss of 2D material even near 1550 nm. We estimate the resulting Q should be in the range of ~1500–1800 (see supplement). The additional Q

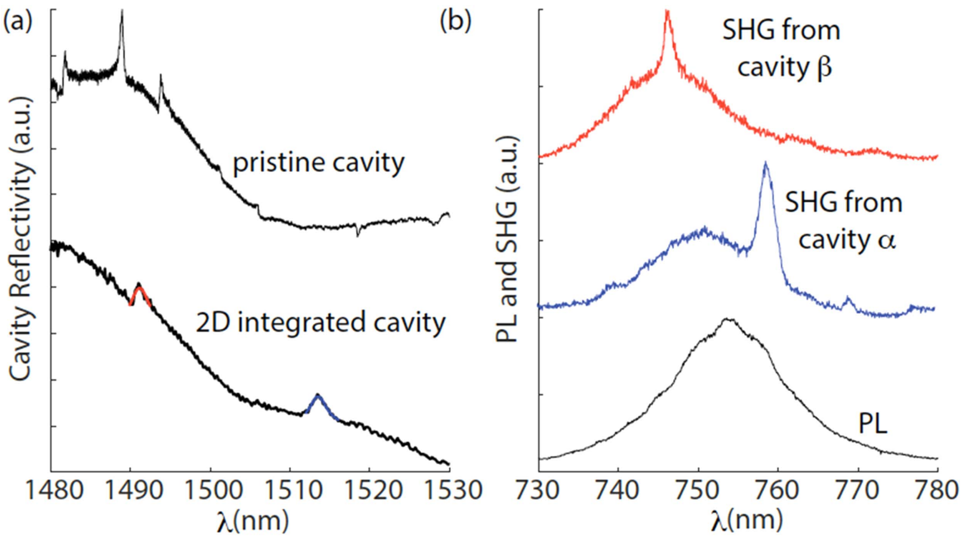


**Figure 2.** Characterization of cavity modes: (a) Cross-polarized reflectivity measurements of the higher order cavity modes before and after monolayer $WSe_2$ transfer. Lorentzian fit is used to estimate the cavity quality factors: blue for the mode '$\alpha$' at ~1515 nm and red for the mode '$\beta$' at ~1490 nm. (b) Overlay of the photoluminescence signal from $WSe_2$ generated via a HeNe laser (black), SHG spectrum from mode $\alpha$ (blue), and SHG spectrum from mode $\beta$ (red). We can clearly identify that the cavity-enhanced SHG peaks occur at half the wavelength of the mode seen in reflectivity. The plots are vertically offset for clarity.

degradation is attributed to the polymer residues from monolayer transfer [22].

## 3. Results

After measuring the linear spectrum of the $WSe_2$ clad cavity, we moved forward to measure the SHG signal (setup is shown in the supplement). We resonantly pumped the cavity using an optical parametric amplifier (Coherent OPA 9800) to generate light near 1500 nm. The pump laser has a repetition frequency of 250 kHz and pulse width of ~200 fs. We conducted all experiments at normal incidence through a 50X Olympus near-IR objective. The incident light was polarization resolved by passing it through a half- and a quarter-wave Fresnel rhomb and remotely controlled linear polarizer before entering the objective. We detected light near the second-harmonic frequency, where we observed background SHG along with a well-defined cavity peak (figure 2(b)). The wavelengths of cavity peaks observed in SHG signal (~745 nm and ~758 nm) correspond exactly to the half of the cavity wavelength observed in reflectivity (~1490 nm and ~1515 nm) (figure 2(a)). These modes are hereby referred to as mode '$\alpha$' (at ~1515 nm) and mode '$\beta$' (at ~1490 nm). We verified that the SHG signal appears only when we pump an area with $WSe_2$, and no signal is observed when we pumped the SOI sample without monolayer $WSe_2$. This rules out any possibility of SHG due to the surface nonlinearity at the silicon-air interface [26]. The interface of silicon and $WSe_2$ provides another interface nonlinearity, however, similar nonlinearity has been measured previously at $MX_2$-$SiO_2$ interfaces and was found to be negligible [14]. A more conclusive signature would have been the characteristic six-fold pattern of polarization-resolved second harmonic signal [27], but due to the strong linear polarization of the cavities, such polarization-resolved measurement could not be performed. However, we pumped a piece of bilayer $WSe_2$ on our silicon chip and found no SHG signal, which suggests the nonlinearity was provided by the monolayer. Note that, the wavelength range, where we observe SHG is similar to the range, where $WSe_2$ PL is (figure 2(b)). Since PL can be generated from the third harmonic of the laser created via silicon, extra care was taken to ensure we indeed measured the cavity peak in the SHG signal. Before measurements we ensured that our observed signal was indeed SHG by tuning the OPA and ensuring that the background signal shifted in response, which could only be the case if the background corresponded to SHG rather than PL. This is the cause of the slight shift in background from the top two SHG measurements in figure 2(b). The PL should have a cubic dependence on the pump power, whereas the measured signal follows a quadratic dependence. Moreover, to observe a cavity signal in PL, we needed to have cavity modes at ~745–758 nm, which was impossible due to the lack of any photonic bandgap in this wavelength range. We also did not observe any such mode under reflectivity, simulation, or PL created by helium-neon laser excitation.

In the rest of the paper, we analyze the mode '$\beta$' while the discussion of mode '$\alpha$' is in the supplementary materials. To extract the cavity contributions, we fit a Lorentzian to the cavity enhanced SHG peak, a Gaussian to the broad SHG spectrum, and a linear polynomial to the non-SHG background (figure 3(a)). The polarization-resolved SHG shows the cavity-enhanced narrow peak is linearly polarized along the

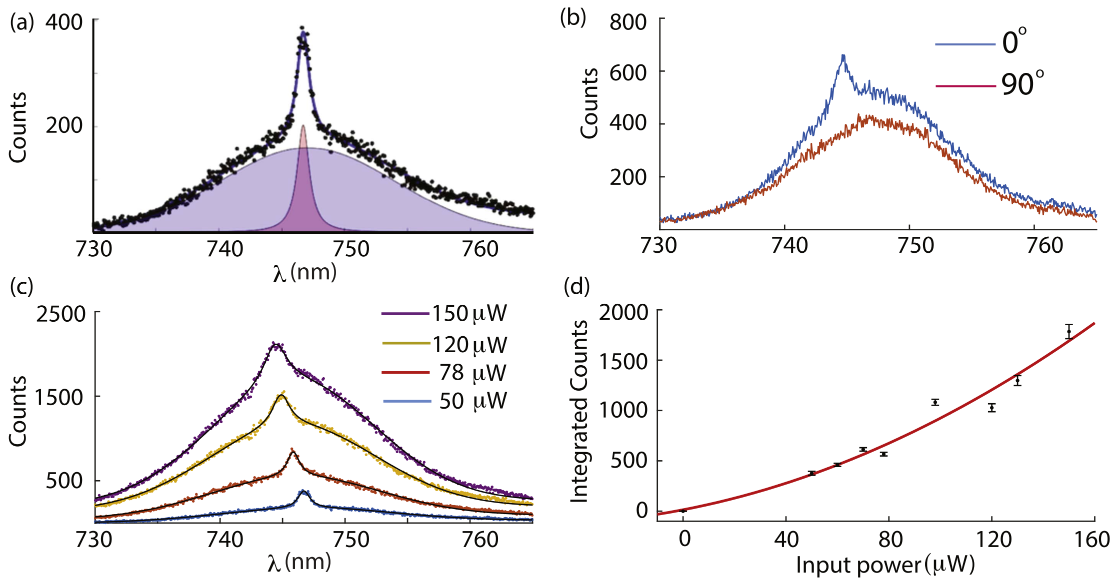


**Figure 3.** Characterization of the second-harmonic signal: (a) A typical SHG spectrum. The total fit is consisted of a Lorentzian for the cavity, a Gaussian curve for the background SHG, and an offset and linear term for the background signal. The corresponding Lorentzian and Gaussian curves are set in to further illustrate their relative contributions to the total fit. (b) Polarization-resolved SHG showing the cavity peak is strongly linearly polarized as expected. (c) Power-dependent (c) SHG spectrum and (d) the cavity-enhanced SHG: each point corresponds to the integrated counts under the Lorentzian fit to the cavity signal. The red line is a quadratic fit.

cavity mode with near unity degree of polarization (figure 3(b)), confirming its coupling to the cavity. We then measured the SHG under different pump powers. Some representative SHG spectra are shown in figure 3(c). All the spectra are also fit with the model described in figure 3(a). A clear blue shift of the cavity resonance was observed, along with a linewidth broadening. We attribute these effects to the free carriers generated by two-photon absorption in silicon [28]. These changes in the cavity parameters are analyzed in detail in the supplementary materials. We plot the area under the Lorentzian fit to the cavity as a function of the input optical power (figure 3(d)). A clear quadratic dependence is observed, validating that this signal is due to SHG. At the lowest pump power (~18 $\mu$W), with the least degradation of the cavity due to free carriers, we found a quality factor of ~630. Theoretically, we expect the $Q$ measured in this fashion to be the same as the $Q$ measured from the linear reflectivity spectrum (~745). We attribute the slight deviation from this estimate to the free carrier induced broadening.

Based on our measurements, we estimated the extent of the cavity enhancement by considering the spectral window defined by the cavity full width half maximum. This convention is chosen as the cavity spectral range is much smaller than that of the background SHG signal. We estimated the relative magnitude of SHG from the measured spectrum by integrating over the cavity spectral window for both the Lorentzian (cavity) and Gaussian fits (the background SHG). Hence the nonlinear conversion efficiency for the bare 2D material is given by the ratio of the area under the Gaussian curve and the incident power. For the cavity, the nonlinear conversion is given by the ratio of the area under the Lorentzian curve and the power coupled to the cavity, which is estimated to be ~1% for our experiment (see supplementary materials). The cavity enhancement is thus given by the ratio of the two conversion efficiencies. We found the enhancement to be ~200 at the lowest pump power, which decreases as a function of the pump power (see supplementary materials). We note that previously reported enhancement with DBR cavities are around a factor of 10, primarily due to the lower quality factor (~100) [18].

## 4. Discussion

Our experiment demonstrated that integrating atomically thin 2D materials onto a photonic crystal cavity results in a two-fold increase in the second-harmonic light in the spectral region of interest. More importantly, we explored a new way to enable second-order non-linear optics in a silicon-compatible platform. We note that the reported enhancement is significantly lower than the theoretical maximum. Partially it is due to that silicon absorbs a significant amount of second-harmonic signal, and the two-photon absorption further degrades the efficiency due to the cavity broadening. In addition, we used a silicon photonic crystal with a mode only at the fundamental frequency. We expect that the SHG can be further enhanced by engineering two cavity modes, one at the fundamental frequency, and the other at the second-harmonic frequency, with good modal overlap between them to ensure phase matching [10, 29]. The theoretical efficiency of the SHG then depends on the quality factors of both cavities $Q_1^2 Q_2$, where $Q_1$ ($Q_2$) is the quality factor of the fundamental (second harmonic) cavity mode. Finally, the slab thickness of the cavity and the cavity material itself may play an important role in the second-harmonic frequency, as recently predicted and also experimentally demonstrated [30, 31]. Especially in the photonic crystal structure, a reduced thickness can increase the field on the cavity surface, albeit at the expense of the quality factor. A more rigorous electromagnetic modelling of 2D material clad cavities is required to find the optimum thickness, where the nonlinear conversion efficiency will be maximized.

## 5. Conclusions

Future devices can substantially improve the overall efficiency by using silicon nitride as the underlying material platform. The addition of another cavity mode at the second-harmonic frequency will also provide a considerable performance enhancement. Realizing multiply resonant cavities with good modal overlap in silicon nitride will enable few-photon nonlinear optics under continuous wave operation, as we recently theoretically reported [16]. In addition, second-order nonlinear devices are important for realizing on-chip optical parametric oscillators [3, 32] and optical bistability [1], as well as exploring fundamental studies, including electromagnetically induced transparency [33].

## Acknowledgments

We thank Mr Richard Bojko and Dr Lukas Chrostowski for helpful discussion about silicon photonic fabrication.

**Author contributions**

A M conceived the idea. J Z fabricated the SOI cavity. T F and C L fabricated the 2D material-cavity device. T F and K S performed the optical characterization. T F wrote the paper with input from everyone. X X and A M supervised the whole project.

**Funding sources**

This work is supported by the National Science Foundation under grant NSF-EFRI-1433496, the Air Force Office of Scientific Research-Young Investigator Program under grant FA9550-15-1-0150, and AFOSR (FA9550-14-1-0277). All of the fabrication was performed at the Washington Nanofabrication Facility (WNF), a National Nanotechnology Infrastructure Network (NNIN) site at the University of Washington, which is supported in part by the National Science Foundation (awards 0335765 and 1337840), the Washington Research Foundation, the M J Murdock Charitable Trust, GCE Market, Class One Technologies and Google.

## References

[1] Gibbs H 1985 *Optical Bistability Controlling Light With Light* (Orlando, FL: Academic)
[2] Marandi A *et al* 2014 Network of time-multiplexed optical parametric oscillators as a coherent Ising machine *Nat. Photon.* **8** 937–42
[3] Witzens J, Baehr-Jones T and Hochberg M 2010 Silicon photonics: on-chip OPOs *Nat. Photon.* **4** 10–2
[4] Vahala K J 2003 Optical microcavities *Nature* **424** 839–46
[5] Trivedi R, Khankhoje U K and Majumdar A 2016 Cavity enhanced second-order nonlinear quantum photonic logic circuits *Phys. Rev. Applied* **5** 054001
[6] Razzari L *et al* 2010 CMOS-compatible integrated optical hyper-parametric oscillator *Nat. Photon.* **4** 41–5
[7] Levy J S *et al* 2010 CMOS-compatible multiple-wavelength oscillator for on-chip optical interconnects *Nat. Photon.* **4** 37–40
[8] Rivoire K *et al* 2009 Second harmonic generation in gallium phosphide photonic crystal nanocavities with ultralow continuous wave pump power *Optics Express* **17** 22609–15
[9] Hochberg M and Baehr-Jones T 2010 Towards fabless silicon photonics *Nat. Photon.* **4** 492–4
[10] Pernice W H P *et al* 2012 Second harmonic generation in phase matched aluminum nitride waveguides and micro-ring resonators *Appl. Phys. Lett.* **100** 223501
[11] Xiong C, Pernice W H P and Tang H X 2012 Low-loss, silicon integrated, aluminum nitride photonic circuits and their use for electro-optic signal processing *Nano Lett.* **12** 3562–8
[12] Wang Q H *et al* 2012 Electronics and optoelectronics of two-dimensional transition metal dichalcogenides *Nat. Nano* **7** 699–712
[13] Seyler K L *et al* 2015 Electrical control of second-harmonic generation in a $WSe_2$ monolayer transistor *Nat. Nano* **10** 407–11
[14] Janisch C *et al* 2014 Extraordinary second harmonic generation in tungsten disulfide monolayers *Sci. Rep.* **4** 5530
[15] Xia F *et al* 2014 Two-dimensional material nanophotonics *Nat. Photon.* **8** 899–907
[16] Majumdar A *et al* 2015 Hybrid 2D material nanophotonics: a scalable platform for low-power nonlinear and quantum optics *ACS Photonics* **2** 1160–6
[17] Yi F *et al* 2016 Optomechanical enhancement of doubly resonant 2D optical nonlinearity *Nano Lett.* **16** 1631–6
[18] Day J, Lee Y-H and Menon V M 2016 Microcavity enhanced second harmonic generation in 2D semiconductors *Conf. on Lasers and Electro-Optics* (San Jose, California: Optical Society of America)
[19] Akselrod G M *et al* 2015 Leveraging nanocavity harmonics for control of optical processes in 2D semiconductors *Nano Lett.* **15** 3578–84
[20] Wu S *et al* 2015 Monolayer semiconductor nanocavity lasers with ultralow thresholds *Nature* **520** 69–72
[21] Sanfeng W *et al* 2014 Control of two-dimensional excitonic light emission via photonic crystal *2D Materials* **1** 011001
[22] Majumdar A *et al* 2013 Electrical control of silicon photonic crystal cavity by graphene *Nano Lett.* **13** 515–8
[23] Lai Y *et al* 2014 Genetically designed L3 photonic crystal nanocavities with measured quality factor exceeding one million *Appl. Phys. Lett.* **104** 241101
[24] Andres C-G *et al* 2014 Deterministic transfer of two-dimensional materials by all-dry viscoelastic stamping *2D Materials* **1** 011002
[25] Englund D *et al* 2010 Resonant excitation of a quantum dot strongly coupled to a photonic crystal nanocavity *Phys. Rev. Lett.* **104** 073904
[26] Ponath H-E and Stegeman G I 1991 *Nonlinear Surface Electromagnetic Phenomena* 1st edn (Amsterdam: Elsevier)
[27] Kumar N *et al* 2013 Second harmonic microscopy of monolayer MoS2 *Phys. Rev.* B **87** 161403
[28] Bristow A D, Rotenberg N and van Driel H M 2007 Two-photon absorption and Kerr coefficients of silicon for 850–2200 nm *Appl. Phys. Lett.* **90** 191104

[29] Lin Z *et al* 2016 Cavity-enhanced second-harmonic generation via nonlinear-overlap optimization *Optica* **3** 233–8

[30] Merano M 2016 Nonlinear optical response of a two-dimensional atomic crystal *Opt. Lett.* **41** 187–90

[31] Zeng J *et al* 2015 Enhanced second harmonic generation of MoS2 layers on a thin gold film *Nanoscale* **7** 13547–53

[32] Martinelli M *et al* 2001 Ultra-low threshold CW triply resonant OPO in the near infrared using periodically poled lithium niobate *J. Opt. A: Pure Appl. Opt.* **3** 300

[33] Zou C, Guo X, Jun H and Tang H 2016 Nonlinear optic induced transparency and frequency conversion on a chip *Frontiers in Optics 2016* OSA Technical Digest (online) (Optical Society of America) paper FTh4G.2